ChemPubSoc Europe

DOI: 10.1002/cssc.201701794

CHEMSUSCHEM Full Papers

Promoting Photocatalytic Overall Water Splitting by Controlled Magnesium Incorporation in $SrTiO_3$ Photocatalysts

Kai Han,[a] Yen-Chun Lin,[a, b] Chia-Min Yang,[b] Ronald Jong,[a] Guido Mul,[a] and Bastian Mei*[a]

$SrTiO_3$ is a well-known photocatalyst inducing overall water splitting when exposed to UV irradiation of wavelengths <370 nm. However, the apparent quantum efficiency of $SrTiO_3$ is typically low, even when functionalized with nanoparticles of Pt or Ni@NiO. Here, we introduce a simple solid-state preparation method to control the incorporation of magnesium into the perovskite structure of $SrTiO_3$. After deposition of Pt or Ni@NiO, the photocatalytic water-splitting efficiency of the Mg:$SrTiO_x$ composites is up to 20 times higher compared to $SrTiO_3$ containing similar catalytic nanoparticles, and an apparent quantum yield (AQY) of 10% can be obtained in the wavelength range of 300–400 nm. Detailed characterization of the Mg:$SrTiO_x$ composites revealed that Mg is likely substituting the tetravalent Ti ion, leading to a favorable surface–space–charge layer. This originates from tuning of the donor density in the cubic $SrTiO_3$ structure by Mg incorporation and enables high oxygen-evolution rates. Nevertheless, interfacing with an appropriate hydrogen evolution catalyst is mandatory and non-trivial to obtain high-performance in water splitting.

Introduction

Photocatalytic water splitting is an attractive method for storage and conversion of solar energy. However, only few semiconductor materials are capable of driving the overall water splitting reaction.[1,2] For GaN:ZnO, when modified with Rh/Cr_2O_3 particles, an apparent quantum yield (AQY) of 5.1% (at 410 nm) has been reported.[3,4] Other effective photocatalysts require excitation by UV light <300 nm.[5,6] An AQY of 56% at 270 nm was reported for La-doped $NaTaO_3$,[5] whereas for Ga_2O_3, AQYs of up to 71% have been achieved.[7–9] Strontium titanate ($SrTiO_3$) has already been used for almost four decades in photocatalytic water splitting,[10–13] and although progress has been slow in increasing the AQY, $SrTiO_3$ is among the few examples that actually facilitates overall water splitting under solar-light illumination, besides the aforementioned GaN:ZnO. $SrTiO_3$ is an ABO_3-type perovskite oxide containing an alkaline-earth cation on the A site and a tetravalent transient-metal cation on the B site.[14] For these structures it is usually accepted that introducing new heteroatoms on either an A or B site will lead to changes in 3d electron interactions, eventually tuning the valence state and electronic structure of the perovskite material.[15,16] For example, through tuning the La^{3+}/Sr^{2+} ratio in $La_{1-x}Sr_xBO_3$ and $La_{1-x}Sr_xBO_4$ (B = Fe, Co, Mn, or Ni) oxides, Patzke and co-workers[17] demonstrated that even a transition from insulating to metal-like behavior can be achieved. Hence, as a typical perovskite oxide, $SrTiO_3$ is susceptible to tuning of its chemical and physical properties by altering its composition.[15,16] Naturally introducing new heteroatoms can also be expected to drastically alter the capabilities of $SrTiO_3$ in photocatalytic water splitting.

Only recently, flux treatment in $SrCl_2$ was used to i) improve the crystallinity of $SrTiO_3$, ii) change the particle morphology, and iii) introduce dopants (mainly Al), thereby significantly increasing the AQY (@360 nm) to 30%.[18–20] At the same time, the same group of researchers reported a similar increase in AQY by simple impregnation of as-prepared $SrTiO_3$ with various metal salts and subsequent diffusion of the metal ion into the $SrTiO_3$ particles by high temperature.[18] Among others, Mg was shown to be a valuable additive, although, as also mentioned by Sakata et al.,[18] a more detailed understanding of the origin of the enhancement in the overall water splitting performance is required.

Here, a simple two-step solid-state preparation method was applied to incorporate Mg into $SrTiO_3$. This two-step approach allowed for a well-controlled metal-ion incorporation and easy adjustment of the Mg content in the semiconductor material. Thus, a rigorous analysis of the effect of Mg doping on i) the phase purity of $SrTiO_3$, ii) the properties and effectivity of different co-catalysts, and iii) the photocatalytic activity in overall

[a] K. Han, Y.-C. Lin, R. Jong, Prof. G. Mul, Dr. B. Mei
Photocatalytic Synthesis Group
MESA+ Institute for Nanotechnology
Faculty of Science and Technology (TNW)
University of Twente
Meander, P.O. Box 217-7500 AE Enschede (The Netherlands)
E-mail: b.t.mei@utwente.nl

[b] Y.-C. Lin, Prof. C.-M. Yang
Department of Chemistry
National Tsing Hua University
Hsinchu 30013 (Taiwan)

Supporting Information and the ORCID identification number(s) for the author(s) of this article can be found under https://doi.org/10.1002/cssc.201701794.

This publication is part of a Special Issue on the topic of Artificial Photosynthesis for Sustainable Fuels. To view the complete issue, visit: http://dx.doi.org/10.1002/cssc.v10.22.

water splitting will be reported. After deposition of an appropriate co-catalyst, such as Pt or Ni@NiO, the photocatalytic overall water splitting (POWS) efficiency is up to 20 times higher compared to the conventional Ni@NiO–$SrTiO_3$ composite. Furthermore, the obtained results clearly demonstrate the importance of controlling the Mg loading well. In particular, different trends in the overall water splitting activity depending on Mg loading and the applied co-catalyst will be discussed.

Results and Discussion

Structural characterization of Mg-modified $SrTiO_3$

Mg-modified $SrTiO_3$ was prepared by a two-step synthesis. After impregnation of rutile TiO_2 with $MgSO_4$ and subsequent annealing, the obtained powder was converted into Mg:$SrTiO_3$ by high-temperature treatment using $SrCO_3$ as strontium source. The composition of the different Mg-modified $SrTiO_3$ materials was first verified by X-ray fluorescence (XRF), yielding the atomic ratios provided in Table 1.

Table 1. Analysis of the Mg content and phase composition of Mg:$SrTiO_x$ materials.

$Sr_x(Mg_yTi)O$	Composition (by XRF)	Phase composition (by XRD)
For $x=y+1$	$Sr_{1.2}Mg_{0.2}TiO_x$ $Sr_{1.25}Mg_{0.3}TiO_x$	pure cubic (Mg:)$SrTiO_3$ phase
For $x>y+1$	$Sr_{1.25}Mg_{0.1}TiO_x$ $Sr_{1.25}Mg_{0.2}TiO_x$	Sr_2TiO_4 (8–40 %) + (Mg:)$SrTiO_3$ (60–92 %) composite
For $x<y+1$	$Sr_{1.25}Mg_{0.5}TiO_x$	rutile TiO_2 (20 %) + (Mg:)$SrTiO_3$ (80 %) composite

Structural analysis of the samples performed by X-ray diffraction (XRD) and Raman spectroscopy is shown in Figure 1. The main diffraction lines of all samples (Figure 1 a), independently of the Mg content, can be assigned to cubic $SrTiO_3$ with orientations of (110), (111), (200), (211), and (220) located at 2θ of 32.58°, 40.1°, 46.61°, 57.9°, and 67.95°, respectively.[21] The XRD pattern of $Sr_{1.25}Mg_{0.3}TiO_x$ indicates that a phase-pure cubic $SrTiO_3$-like material was obtained. Generally, the full width at half maximum (FWHM) of the (110) diffraction line hardly changes. From the FWHM of the (110) diffraction line of 0.19–0.36, primary crystal size ranges can be estimated to range from 10 to 20 nm. For non-stoichiometric ratios of (Mg + Ti):Sr < 1, as in $Sr_{1.25}Mg_{0.1}TiO_x$ and $Sr_{1.25}Mg_{0.2}TiO_x$, diffraction lines at 31.6° and 43.9° are additionally observed, which can be assigned to the tetragonal Sr_2TiO_4 phase.[22]

Alternatively, for samples exceeding the stoichiometric ratio [(Mg + Ti):Sr > 1], non-converted rutile TiO_2 is observed, in addition to cubic $SrTiO_3$. Based on these observations and as the ionic radii of Mg^{2+} (72 pm) and Ti^{4+} (74 pm) are comparable, we conclude that Mg is likely to substitute Ti in the lattice.

To further explore structural changes induced by Mg incorporation into $SrTiO_3$, Raman spectroscopy was employed (Figure 1 b). Comparison with measured reference spectra of tetragonal Sr_2TiO_4 and rutile TiO_2 (Figure S1) validate that Raman assignments are in agreement with phase identification by XRD. Only for materials with near-stoichiometric molar ratios of (Mg + Ti):Sr, the typical second-order broad bands at 200–400 cm^{-1} and 600–800 cm^{-1} for $SrTiO_3$ in its cubic structure are obtained,[22,23] whereas Sr_2TiO_4 or rutile TiO_2 can be clearly identified in Raman spectra of non-stoichiometric compositions.

For comparison, MgO-loaded $SrTiO_3$ was prepared by impregnation of as-prepared $SrTiO_3$ with $MgSO_4$. In contrast to the Mg-modified $SrTiO_3$ materials, the diffraction lines of $SrTiO_3$ are dominant, and only the characteristic Raman bands of $SrTiO_3$ are observed (Figure S2), indicating that on-surface deposited MgO did not alter the cubic structure of $SrTiO_3$. The normalized intensities above 1000 cm^{-1} are likely owed to residual sulphate in this sample (Figure S2).

High-resolution scanning electron microscopy (Figure S3) and UV/Vis diffuse reflectance spectroscopy (Figure S4) were used to investigate the morphology and optical properties, that is, the band gap of the prepared Mg-modified $SrTiO_3$ materials. In agreement with XRD and Raman spectroscopy, similar particle morphologies, that is, crystals with multiple facets, were observed for phase-pure Mg:$SrTiO_3$. For composite structures such as $Sr_{1.25}Mg_{0.2}TiO_x$ consisting of $SrTiO_3$ and Sr_2TiO_4 phases, particles with smooth extended facets are also observed. Likewise, using Tauc plots, a slightly larger indirect

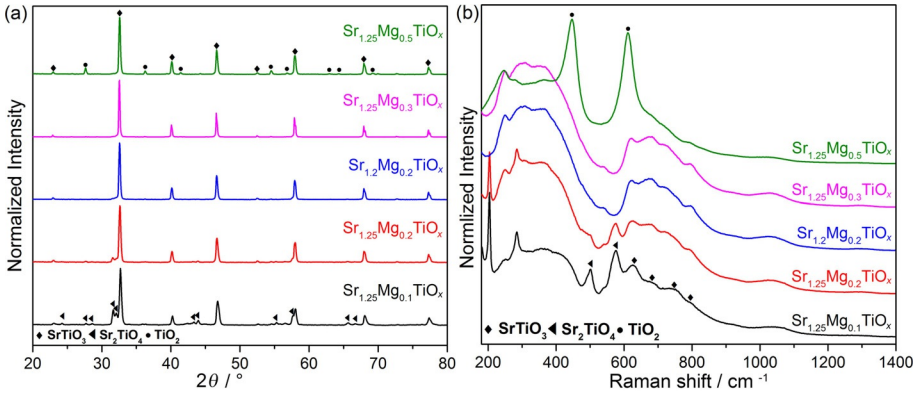

Figure 1. a) XRD patterns and b) Raman spectra of Mg-modified $SrTiO_3$ with different Mg ammounts. Contributions of the $SrTiO_3$ phase (filled square), Sr_2TiO_4 phase (filled triangle), and TiO_2 phase (filled circle) are indicated in each figure.

band gap is estimated for mixed-phase Mg-modified $SrTiO_x$ materials (3.2 eV), compared to the pure-phase sample $Sr_{1.25}Mg_{0.3}TiO_x$ (band gap of 3.1 eV), which is in agreement with the generally larger band gap of Sr_2TiO_4 (Figure S4 b).

Overall water splitting performance

The photocatalytic activity of the prepared materials was tested after applying suitable co-catalysts.

Here, Pt and Ni@NiO core–shell structures were used, as these co-catalysts were previously reported to facilitate photocatalytic overall water splitting (POWS) of $SrTiO_3$.[24,25] The Ni@NiO loading was found to be optimal at 1 wt% for $SrTiO_3$ and $Sr_{1.25}Mg_{0.2}TiO_x$ (see Figure 2 a). Hence, all Mg-modified $SrTiO_x$ materials were modified with the optimized Ni@NiO loading of 1 wt% and subsequently tested for overall water splitting in a continuously stirred tank reactor (CSTR) under solar-light illumination. The evolution rates of H_2 and O_2 were measured with a micro-gas chromatograph (micro-GC) equipped with a pulsed discharge detector (PDD). Here, all measurements were performed with a purge-gas flow rate of 10 mL min^{-1}. It should be noted that the back reaction of H_2 and O_2 to water might be suppressed by the flow of the purge gas, and optimization of the purge-gas flow could lead to close-to-complete prevention of this back reaction.[26] We currently evaluate the effect of purge-gas rate, light intensity, reactor geometry, and catalyst concentration on the performance of our photocatalytic flow reactor in water splitting and oxidation of H_2 to H_2O.

As previously shown for Ni@NiO-modified $SrTiO_3$,[25] transients in H_2 and O_2 evolution are observed for all Mg-modified $SrTiO_3$ materials. Typical transient evolution curves for hydrogen and oxygen obtained with Ni@NiO-modified $Sr_{1.25}Mg_{0.3}TiO_x$ are shown in Figure 2 b (for further information about the transient evolution of H_2 and O_2 with the other Mg-modified $SrTiO_3$, as well as different reference materials see the Supporting Information; Figures S5 and S6). Thus, for Ni@NiO-modified $Sr_{1.25}Mg_{0.2}TiO_x$, a peak in both H_2 and O_2 evolution rate was obtained after 30 min of testing, and only after three hours of continuous testing, close to steady state, catalytic evolution rates of H_2 and O_2 were measured. We tentatively assign the transients to changes in the Ni@NiO structure and presumably the oxidation state of Ni, which is in agreement with our recent results for Ni@NiO-modified $SrTiO_3$.[25]

Although the transient behavior of the Ni@NiO co-catalysts has to be further explored (for further information see the Supporting Information and Figure S6), a clear improvement in the POWS after Mg modification of $SrTiO_3$ is obtained. Peak efficiencies as well as steady-state rates suggest that a small Mg content drastically improves the performance of the composite photocatalysts. Furthermore, the photocatalytic data reveal that the highest POWS are obtained for materials with a fully maintained $SrTiO_3$ phase (Figure 3). For the Ni@NiO-modified $Sr_{1.25}Mg_{0.3}TiO_x$ photocatalyst, H_2 peak and steady-state efficiencies of 8.8 μmol g^{-1} min^{-1} and 1.2 μmol g^{-1} min^{-1} were obtained, respectively, resulting in a state-of-the-art apparent quantum efficiency of 9.1% in steady-state conditions, at a ratio of H_2 and O_2 close to 2:1 (since Mg:$SrTiO_3$ absorbs light below 400 nm, we estimated the AQY using intensities in the wavelength range of 300–400 nm as emitted by the solar simulator; see the Supporting Information and Figure S7). In comparison to Ni@NiO-$SrTiO_3$ or Ni@NiO-modified MgO-loaded $SrTiO_3$, a 20 times higher steady-state efficiency was obtained (Figure 3 a). It should be noted that the reported transients for Ni@NiO-$SrTiO_3$ and Ni@NiO-modified MgO-loaded $SrTiO_x$ can only be visualized owing to the time resolution of our micro-GC, and sensitivity toward H_2 and O_2 provided by the PDD. Usually, these initial changes in the H_2 and O_2 evolution rates are not observed when using batch reactors connected to GCs with thermal conductivity detector (TCD) detectors, typically allowing the first measurement only after 1 h of illumination. Our future work is dedicated to stabilizing the initial rates induced by the Ni@NiO-Mg:$SrTiO_x$ composites.

For samples with high Mg loadings, such as in $Sr_{1.25}Mg_{0.5}TiO_x$, the performance is significantly lower (Figure 3 a). The photocatalytic performance of pure Sr_2TiO_4, $Mg_{0.2}TiO_x$, and mixtures of Sr_2TiO_4/$SrTiO_3$ is also low and none of these samples show a comparable activity to the Mg:$SrTiO_3$ photocatalysts (Figure S8). We therefore exclude possible effects of novel phases and conclude that Sr_2TiO_4 and $Mg_{0.2}TiO_x$ are inactive for POWS.

As for Ni@NiO-modified composite materials, significantly higher POWS were obtained for Mg-modified $SrTiO_3$ materials

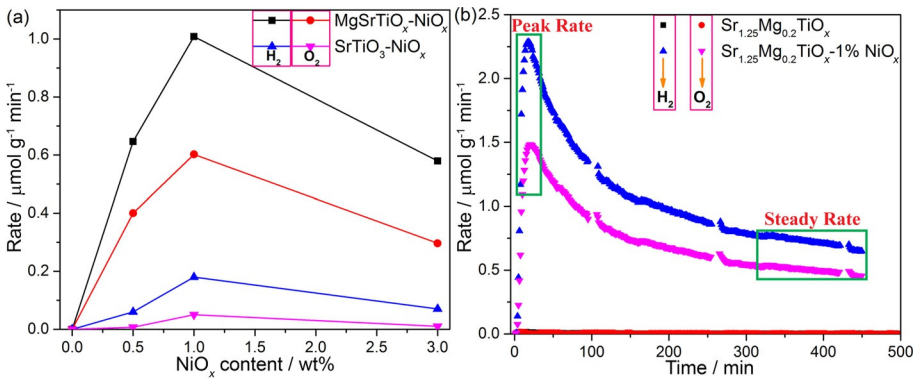

Figure 2. Photocatalytic performance in H_2 and O_2 evolution under solar light. a) Optimization of NiO_x loading for $SrTiO_3$ and $Sr_{1.25}Mg_{0.2}TiO_x$, b) comparison of the photocatalytic transient of Ni@NiO-modified $Sr_{1.25}Mg_{0.2}TiO_x$ and unmodified $Sr_{1.25}Mg_{0.2}TiO_x$. Time intervals to determine the peak, and steady-state rates in H_2 and O_2 production are highlighted.

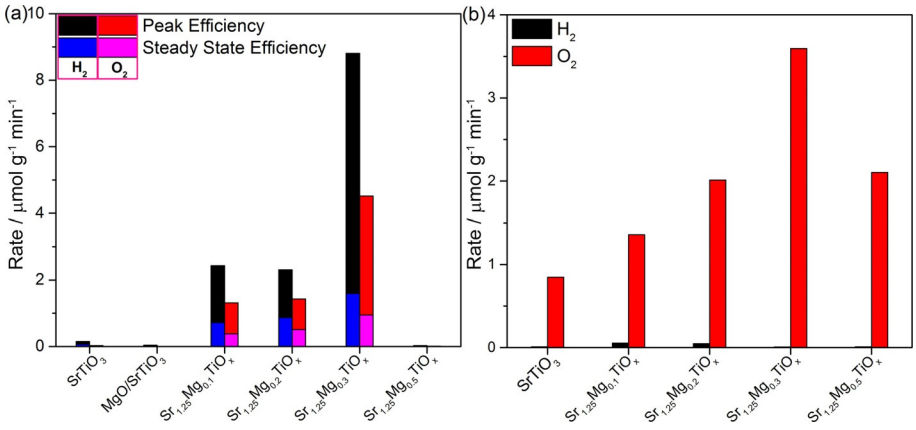

Figure 3. Photocatalytic efficiency in H_2 and O_2 evolution under solar light. a) Photocatalytic behavior for different Mg ratio with 1 wt% NiO_x modification, b) photocatalytic half reaction with sacrificial agent (2 mM $FeSO_4$ for H_2 evolution and 2 mM $Fe_2(SO_4)_3$ for O_2 evolution).

compared to bare $SrTiO_3$ photocatalysts after photodeposition of 0.5 wt% Pt (Table 2 and Figures S9–S12). In contrast to the Ni@NiO-modified composite materials, however, steady-state rates were obtained within a short-time period of solar illumination. Again, the samples with relatively high Mg content performed significantly worse compared to those of low Mg content, and the mixed-phase $Mg_{0.1}Sr_{1.25}TiO_x$ catalyst showed the highest POWS activity. After Pt deposition, grey powders of $SrTiO_3$ and $Mg_{0.1}Sr_{1.25}TiO_x$ were obtained (Figure S13), as expected for materials with metallic Pt, whereas the samples with higher Mg content were slightly yellow, evidencing the deposition of Pt in a higher oxidation state.[24]

To evaluate the surface reactivity of Mg:$SrTiO_x$, we tested the efficiency of the materials for H_2 and O_2 evolution using sacrificial agents (Figure 3b), namely $FeSO_4$ and $Fe_2(SO_4)_3$. As shown in Figure 3b, the presence of Mg in the $SrTiO_3$ structure has a strong influence on the water oxidation activity, and the measured O_2 evolution rates follow the trends observed for Mg-modified $SrTiO_x$ with Ni@NiO co-catalysts in overall water splitting. Indeed, the O_2 evolution rates closely resemble the measured peak efficiencies with Ni@NiO-$Sr_{1.25}Mg_{0.3}TiO_x$. For proton reduction to H_2, however, Mg:$SrTiO_x$ shows little activity, indicating that Pt or Ni@NiO are necessary for this half reaction.

Table 2. Photocatalytic water splitting performance of the various Mg-modified $SrTiO_x$ with Ni@NiO or Pt co-catalysts.

Sample	Co-catalyst	H_2 [nmol min^{-1}]	O_2 [nmol min^{-1}]
$SrTiO_3$	1 wt% Ni@NiO	1.8[a]/3.8[b]	0.251[a]/0.8[b]
$Mg_{0.1}Sr_{1.25}TiO_x$	1 wt% Ni@NiO	18 [a]/57.8[b]	9.5[a]/32.8[b]
$Mg_{0.2}Sr_{1.25}TiO_x$	1 wt% Ni@NiO	21.8[a]/57.8[b]	12.5[a]/35.8[b]
$Mg_{0.3}Sr_{1.25}TiO_x$	1 wt% Ni@NiO	39.8[a]/220.3[b]	22.8[a]/113[b]
$Mg_{0.5}Sr_{1.25}TiO_x$	1 wt% Ni@NiO	0.5[a]/0.63[b]	0.18[a]/2[b]
$SrTiO_3$	0.5 wt% Pt	0.5	0.3
$Mg_{0.1}Sr_{1.25}TiO_x$	0.5 wt% Pt	10.8	6.3
$Mg_{0.2}Sr_{1.25}TiO_x$	0.5 wt% Pt	7.8	4.3
$Mg_{0.3}Sr_{1.25}TiO_x$	0.5 wt% Pt	0.5	1.3
$Mg_{0.5}Sr_{1.25}TiO_x$	0.5 wt% Pt	0.005	0.5

[a] Steady-state rate. [b] Peak rate.

Based on all our observations, we conclude that phase-pure, cubic Mg:$SrTiO_x$ is a favorable material for POWS. The activity is likely owed to the beneficial influence of Mg on the electronic structure of $SrTiO_3$, combined with high catalytic activity for O_2 evolution, whereas a suitable H_2 evolution catalyst is required for high performance in POWS.

Mg modification: effects on the electronic structure

To better understand the band structure and charge separation of Mg-modified $SrTiO_x$, photoelectrodes of the Mg:$SrTiO_x$ composites were prepared (without co-catalyst, Figure S14) and Mott–Schottky analysis was applied (Figure 4), using the following Mott–Schottky relation [Eq. (1)]:

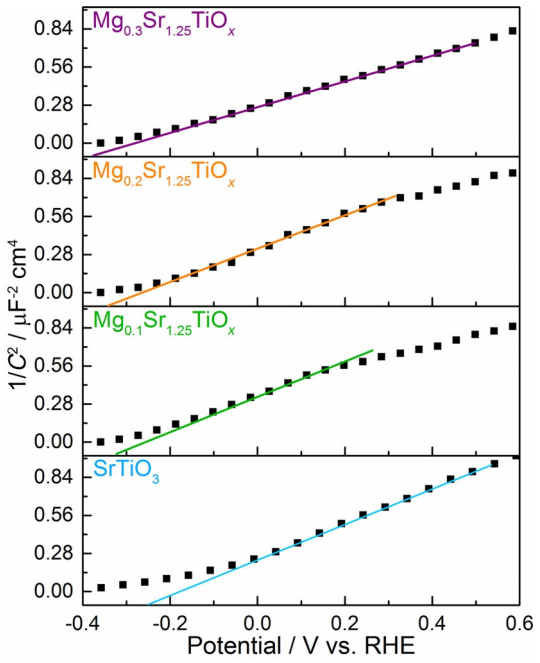

Figure 4. Mott–Schottky curves of Mg:$SrTiO_x$ with different Mg loadings obtained at 2.5 kHz in 0.5 M Na_2SO_4.

$$\frac{1}{C_{SC}^2} = \frac{2}{e\varepsilon\varepsilon_0 N}\left(E_{appl} - E_{fb} - \frac{KT}{e}\right) \quad (1)$$

where C_{sc} is the capacitance of the space-charge layer, e is the charge of the electron, ε is the dielectric constant of the semiconductor (300 for $SrTiO_3$)[27,28], ε_0 is the vacuum permittivity of free space, N is the donor density (electron donor concentration for an n-type semiconductor or hole acceptor concentration for a p-type semiconductor), E_{appl} is the applied potential, E_{fb} is the flat-band potential, k is the Boltzmann constant, and T is the absolute temperature. The flat-band potential (E_{fb}) and donor intensity (N) were calculated and are summarized in Table 3.[10,11] Additionally, the conduction-band potential (E_{CB}) and the depletion layer thickness (W_o) obtained from Equations (2) and (3) are included.

Table 3. Summary of the obtained Mott–Schottky results for $SrTiO_3$ and Mg:$SrTiO_x$ materials with different Mg content.

Sample	E_{fb} [V_{RHE}]	E_{CB} [V_{RHE}]	N [cm^{-3}]	W_o [nm]
$SrTiO_3$	−0.25	−0.3	4.82×10^{19}	26
$Mg_{0.1}Sr_{1.25}TiO_x$	−0.31	−0.39	1.27×10^{19}	51
$Mg_{0.2}Sr_{1.25}TiO_x$	−0.33	−0.41	1.26×10^{19}	51
$Mg_{0.3}Sr_{1.25}TiO_x$	−0.34	−0.41	1.61×10^{19}	45

$$E_{CB} = E_{fb} + \frac{kT}{e}\ln\left(\frac{N}{N_c}\right) \quad (2)$$

$$W_o = \left(\frac{2\varepsilon\varepsilon_0}{eN}\right)^{1/2} \quad (3)$$

N_c is the effective density of states in the conduction band, which is roughly estimated to be 2.8×10^{20} cm^{-3} for $SrTiO_3$.[29]

Although generally in agreement with previous reports,[12] the Mott–Schottky analysis reveals that the donor density of Mg:$SrTiO_x$ is significantly lower compared to the unmodified $SrTiO_3$ sample, which is in good agreement with earlier impedance measurements on Ho-modified $SrTiO_3$ photoelectrodes and first principle calculations on Mg-modified TiO_2 hollow spheres.[30,31] The slight increase in donor density observed for the phase-pure $Mg_{0.3}Sr_{1.25}TiO_x$ might be related to the Sr_2TiO_4 phases present in the $Mg_{0.1}Sr_{1.25}TiO_x$ and $Mg_{0.2}Sr_{1.25}TiO_x$ materials. Furthermore, the calculations suggest that the conduction-band position is moved slightly upwards to more negative potentials and that the depletion-layer thickness increases. For a wide band-gap semiconductor, the depletion-layer thickness (W_0) is of major importance, as this determines surface-confined effective charge separation, and hence improves light utilization (Scheme 1).

Thus, for a depletion-layer thickness equal to the penetration depth of incident light, maximum photocatalytic efficiencies can be expected.[32–34] It should be noted that in contrast to other studies in which an intrinsically n-type doped material was converted into a p-type semiconductor through Mg modification,[35,36] all samples prepared herein demonstrate n-type behavior (Figure 4). Electrodes prepared from powdered materials are far from ideal for Mott–Schottky analysis and certainly a systematic impedance analysis using more comprehensive models and better defined Mg:$SrTiO_x$ films are indispensable to use the full potential of the Mott–Schottky analysis. Nonetheless, the Mott–Schottky and photoelectrochemical analysis (see Figure S14) are in good agreement with the catalytic data shown for the Ni@NiO- and Pt-modified materials. The improved performance can likely be assigned to a favorable (surface) electronic structure of the Mg-modified $SrTiO_x$ materials and to a cathodic shift of the E_{fb} associated with a larger space charge layer.

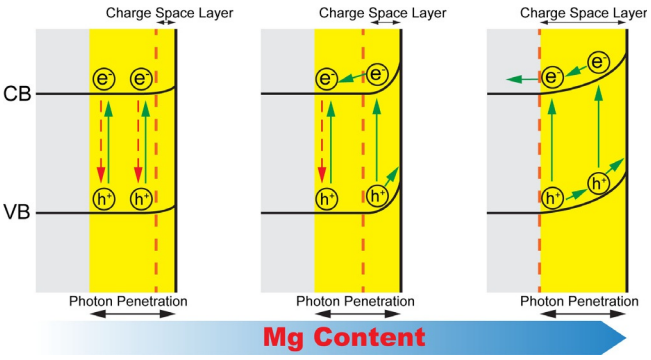

Scheme 1. Summary of the effect of Mg incorporation into $SrTiO_3$ on the electronic structure of the synthesised materials.

It is expected that further increases in POWS can be achieved by slightly modifying the donor density, however, special care has to be taken when modifying the obtained materials with the required co-catalysts. Based on the results obtained with Ni@NiO co-catalysts, the highest POWS can be achieved with the phase-pure $Mg_{0.3}Sr_{1.25}TiO_x$. For Pt-modified samples with increasing Mg content, a similar trend is observed. However, the phase-pure $Mg_{0.3}Sr_{1.25}TiO_x$ sample is hardly active, evidencing that the interface between the photodeposited Pt particles is not favorable and/or that Pt is present in an oxidized state; the oxide being less suitable to drive the H_2 evolution reaction. In the presence of H_2-evolving active metallic Pt nanoparticles (even trace amounts might be sufficient)[37,38], we expect a similar activity increase, as observed for the Ni@NiO-modified $Mg_{0.3}Sr_{1.25}TiO_x$ composite. Future studies will be mainly focused on stabilizing the high initial (peak) activity of the Ni@NiO-modified phase-pure $Mg_{0.3}Sr_{1.25}TiO_x$ material and the development of alternative co-catalysts providing long-term stability during POWS.[39]

Conclusions

Here, a simple solid-state method was applied to prepare Mg-modified $SrTiO_x$ photocatalysts. As shown by structural characterization, variation of the Mg content results in the synthesis of materials consisting of various phases. Only for a stoichiometric ratio of (Mg + Ti):Sr, phase-pure cubic $SrTiO_3$ materials were obtained. After deposition of suitable co-catalysts, like Ni@NiO or Pt, the synthesized materials showed dramatic improvement in the photocatalytic overall water splitting (POWS) rates compared to unmodified $SrTiO_3$. Among all the

Mg-modified $SrTiO_x$ samples tested, the phase-pure material, $Sr_{1.25}Mg_{0.3}TiO_x$, provided the highest steady-state apparent quantum yield of 9.1% using solar-light illumination (300–400 nm). Any effect of other phases present in minor quantities on the POWS were ruled out by a series of reference measurements. Using Mott–Schottky measurements and photocatalytic test reactions with sacrificial agents, the beneficial effect of Mg is assigned to extension of the depletion layer (from 25 to 50 nm), allowing for better O_2 evolution capabilities of the Mg-modified $SrTiO_x$ materials. On the other hand, electron transfer to the surface is limited and an appropriate interface with a H_2 evolution catalysts needs to be formed to drive the overall water splitting reaction. Among the co-catalysts tested, Ni@NiO, in an optimized Ni@NiO loading of 1 wt%, seems to perform better than Pt.

Experimental Section

Materials preparation

Bulk $SrTiO_3$ was prepared by a well-known high-temperature treatment of stoichiometric amounts of $SrCO_3$ (99.995%, Sigma–Aldrich) and TiO_2 (rutile phase: 99.995%, Sigma–Aldrich).[24,25] The compounds were thoroughly mixed and subsequently calcined at 1100 °C for 10 h. Mg incorporation into $SrTiO_3$ was achieved by a two-step high-temperature method. First, rutile TiO_2 was impregnated with an aqueous $MgSO_4$ solution using a predefined molar ratio of Mg/Ti. The solution was evaporated to dryness and the powder was calcined in air at 800 °C for 2 h. Afterwards, the powder was thoroughly rinsed with water (at least four times), to remove residual (Mg) sulfate, as verified by Raman spectroscopy (see Figure S2). Then, the obtained $MgTiO_x$ material was mixed with stoichiometric amounts of $SrCO_3$ and calcined at 1100 °C for 10 h to obtain targeted products. These materials are referred to as $Sr_{1.25}Mg_{0.1}TiO_x$, $Sr_{1.25}Mg_{0.2}TiO_x$, $Sr_{1.2}Mg_{0.2}TiO_x$, $Sr_{1.25}Mg_{0.3}TiO_x$, and $Sr_{1.25}Mg_{0.5}TiO_x$. For comparison, a MgO-loaded $SrTiO_3$ was prepared by impregnation of the as-prepared bulk $SrTiO_3$ in an aqueous solution of $MgSO_4$ (molar ration of 0.2). After drying, the obtained powder was calcined at 800 °C for 2 h in air. Modification of the prepared semiconductor materials by core–shell Ni@NiO particles was achieved as previously reported.[25] Briefly, the respective semiconductor powder (0.2 g) was dispersed in an aqueous solution of $Ni(NO_3)_2$ (20 mL). The obtained mixture was stirred for 2 h, subsequently, the solution was evaporated to dryness at 80 °C overnight, and finally the obtained powder was calcined for 1 h at 400 °C in a tube furnace (30 mL min^{-1} synthetic air; heating rate 10 K min^{-1}). After cooling down to room temperature in N_2, the material was reduced for 10 h at 500 °C in a gas mixture of 5% H_2/N_2 (heating rate 10 K min^{-1}; flow 80 mL min^{-1}). The final product was obtained by cooling down in N_2 flow to 130 °C, and a treatment of 1 h in flowing air (30 mL min^{-1}) at this temperature. Photodeposition was applied to deposit Pt nanoparticles on the surface of Mg-modified $SrTiO_x$. Typically, the prepared material (0.2 g) was dispersed into H_2PtCl_6 solution (20 mL) and then exposed to UV light (360–380 nm, 3.21 mW cm^{-2}) for 5 h. Afterwards, the powder was centrifuged and dried at 80 °C overnight.

Sample characterization

XRD measurements were performed on a Bruker D2 (CuK_α source) diffractometer. The phase composition of the different materials was obtained using the Highscore Plus software. Raman spectroscopy (Bruker Senterra) was performed at room temperature with a 532 nm green laser (2 mW). A Philips PW 1480 spectrometer was used for XRF analysis. UV/Vis diffuse reflectance spectra (DRS) were recorded with a UV/Vis spectrophotometer (Thermo Scientific, Evolution 600), the reflectance data were converted to Kulbelka–Munk plots and the corresponding Tauc plots. A Nova 600 Nanolab HR-SEM (FEI instruments) was used for SEM experiments. Mott–Schottky measurements were conducted in a three-electrode setup (using a Biologic VSP Potentiostat) using aerated 0.5 M Na_2SO_4 as electrolyte. Photoelectrochemical measurements were performed in degassed 0.5 M $Na_2SO_4 + Na_2SO_3$ (pH 7.1). A Xe lamp with AM 1.5G filter was used as light source at an intensity of 1.5 suns using back-side illumination. The Mg-modified $SrTiO_x$ working electrode was prepared by electrophoretic deposition of the corresponding powder on an fluorine-doped tin oxide (FTO) substrate.[40] Briefly, electrophoretic deposition was done in a two-electrode configuration in acetone solution (10 mL) with iodine (15 mg) dissolved in the solution. By applying a bias of 40 V for 3 min between the FTO substrate and a Pt electrode, the powder was deposited.

Photocatalytic activity measurements

The photocatalytic activity of the compounds was measured using a CSTR connected to a highly sensitive gas chromatograph (CompactGC Interscience). The GC was equipped with a PDD. By a constant He (7 N) purge (10 mL min^{-1}; in these conditions, back-reaction of H_2 and O_2 is limited/suppressed due to the low H_2 and O_2 partial pressures), the gas to be analyzed was transferred to the GC. In the GC, a 50 μL sample loop inserted a sample onto a Q-bond column to remove H_2O, and a Molsieve 5A to separate the gaseous components present in the sample (H_2, O_2, and N_2). The optical glass reactor (402.013-OG, Hellma) was illuminated by a AM 1.5G solar simulator (ABET technologies model 10500 low-cost solar simulator, 4.9 cm^2 beam area), which is representative of the intensity profile of solar radiation (Figure S15). The incident intensity on the reactor window from 300 to 900 nm amounted to 59 mW cm^{-2}, and from 300 to 400 nm amounted to 0.9 mW cm^{-2}. The measurements were performed using 25 mg catalyst in 25 mL of ultrapure water. After immersion of the photocatalyst, the pH of the solution was measured to be 9. Half-reaction measurements were performed with the unmodified Mg:$SrTiO_x$ materials (no co-catalyst) by adding the corresponding sacrificial agents (2 mM $FeSO_4$ for H_2 evolution and 2 mM $Fe_2(SO_4)_3$ for O_2 evolution) to the prepared photocatalyst slurry solution.

Acknowledgements

The Chinese Science Council is gratefully acknowledged for financially supporting K.H. Y.-C.L. gratefully acknowledges funding from the ERASMUS MUNDUS EURASIACAT project (Advanced Education European-Asiatic Exchange Programme in Materials Science and Catalysis, with ref. nr. 552067). Furthermore, we would like to acknowledge Dr. Rico Keim for performing the analysis of the samples by Scanning and Transmission Electron Microscopy.

Conflict of interest

The authors declare no conflict of interest.

Keywords: electronic structure · magnesium · photocatalysis · strontium titanate · water splitting

[1] T. Hisatomi, J. Kubota, K. Domen, *Chem. Soc. Rev.* **2014**, *43*, 7520 – 7535.
[2] D. M. Fabian, S. Hu, N. Singh, F. A. Houle, T. Hisatomi, K. Domen, F. E. Osterloh, S. Ardo, *Energy Environ. Sci.* **2015**, *8*, 2825 – 2850.
[3] K. Maeda, H. Hashiguchi, H. Masuda, R. Abe, K. Domen, *J. Phys. Chem. C* **2008**, *112*, 3447 – 3452.
[4] K. Maeda, K. Domen, *J. Phys. Chem. Lett.* **2010**, *1*, 2655 – 2661.
[5] H. Kato, K. Asakura, A. Kudo, *J. Am. Chem. Soc.* **2003**, *125*, 3082 – 3089.
[6] K. Maeda, *J. Photochem. Photobiol. C* **2011**, *12*, 237 – 268.
[7] G. W. Busser, B. Mei, P. Weide, P. C. K. Vesborg, K. Stührenberg, M. Bauer, X. Huang, M.-G. Willinger, I. Chorkendorff, R. Schlögl, M. Muhler, *ACS Catal.* **2015**, *5*, 5530 – 5539.
[8] Y. Sakata, Y. Matsuda, T. Nakagawa, R. Yasunaga, H. Imamura, K. Teramura, *ChemSusChem* **2011**, *4*, 181 – 184.
[9] Y. Sakata, T. Hayashi, R. Yasunaga, N. Yanaga, H. Imamura, *Chem. Commun.* **2015**, *51*, 12935 – 12938.
[10] F. Cardon, W. P. Gomes, *J. Phys. D* **1978**, *11*, L63 – L67.
[11] R. De Gryse, *J. Electrochem. Soc.* **1975**, *122*, 711.
[12] I. Watanabe, Y. Matsumoto, E.-I. Sato, *J. Electroanal. Chem. Interfacial Electrochem.* **1982**, *133*, 359 – 366.
[13] T. K. Townsend, N. D. Browning, F. E. Osterloh, *ACS Nano* **2012**, *6*, 7420 – 7426.
[14] J. Shi, L. Guo, *Prog. Nat. Sci. Mater. Int.* **2012**, *22*, 592 – 615.
[15] C. Yu, Y. Shimizu, H. Arai, *Sens. Actuators* **1988**, *14*, 309 – 318.
[16] W. Zeng, T. M. Liu, C. L. Lv, D. J. Liu, *Phys. B* **2011**, *406*, 1420 – 1428.
[17] H. Liu, R. Moré, H. Grundmann, C. Cui, R. Erni, G. R. Patzke, *J. Am. Chem. Soc.* **2016**, *138*, 1527 – 1535.
[18] Y. Sakata, Y. Miyoshi, T. Maeda, K. Ishikiriyama, Y. Yamazaki, H. Imamura, Y. Ham, T. Hisatomi, J. Kubota, A. Yamakata, K. Domen, *Appl. Catal. A* **2016**, *521*, 227 – 232.
[19] H. Kato, M. Kobayashi, M. Hara, M. Kakihana, *Catal. Sci. Technol.* **2013**, *3*, 1733.
[20] Y. Ham, T. Hisatomi, Y. Goto, Y. Moriya, Y. Sakata, A. Yamakata, J. Kubota, K. Domen, *J. Mater. Chem. A* **2016**, *4*, 3027 – 3033.
[21] G. Zhang, W. Jiang, S. Hua, H. Zhao, L. Zhang, Z. Sun, *Nanoscale* **2016**, *8*, 16963 – 16968.
[22] Y. S. Jia, S. Shen, D. G. Wang, X. Wang, J. Y. Shi, F. X. Zhang, H. X. Han, C. Li, *J. Mater. Chem. A* **2013**, *1*, 7905 – 7912.
[23] F. A. Rabuffetti, H.-S. Kim, J. A. Enterkin, Y. Wang, C. H. Lanier, L. D. Marks, K. R. Poeppelmeier, P. C. Stair, *Chem. Mater.* **2008**, *20*, 5628 – 5635.
[24] M. G. C. Zoontjes, K. Han, M. Huijben, W. G. van der Wiel, G. Mul, *Catal. Sci. Technol.* **2016**, *6*, 7793 – 7799.
[25] K. Han, T. Kreuger, B. Mei, G. Mul, *ACS Catal.* **2017**, *7*, 1610 – 1614.
[26] M. Qureshi, K. Takanabe, *Chem. Mater.* **2017**, *29*, 158 – 167.
[27] Note that the dielectric constant might change with composition.
[28] T. Ming, J. Suntivich, K. J. May, K. A. Stoerzinger, D. H. Kim, Y. Shao-Horn, *J. Phys. Chem. C* **2013**, *117*, 15532 – 15539.
[29] M. Ahrens, R. Merkle, B. Rahmati, J. Maier, *Phys. B* **2007**, *393*, 239 – 248.
[30] L. Zhao, L. Fang, W. Dong, F. Zheng, M. Shen, T. Wu, *Appl. Phys. Lett.* **2013**, *102*, 121905.
[31] L. Gao, Y. Li, J. Ren, S. Wang, R. Wang, G. Fu, Y. Hu, *Appl. Catal. B* **2017**, *202*, 127 – 133.
[32] A. J. Bard, *J. Photochem.* **1979**, *10*, 59 – 75.
[33] A. N. Pinheiro, E. G. S. Firmiano, A. C. Rabelo, C. J. Dalmaschio, E. R. Leite, *RSC Adv.* **2014**, *4*, 2029 – 2036.
[34] Z. Zhang, J. T. Yates, *Chem. Rev.* **2012**, *112*, 5520 – 5551.
[35] J. Yang, D. Wang, H. Han, C. Li, *Acc. Chem. Res.* **2013**, *46*, 1900 – 1909.
[36] M. G. Kibria, S. Zhao, F. A. Chowdhury, Q. Wang, H. P. T. Nguyen, M. L. Trudeau, H. Guo, Z. Mi, *Nat. Commun.* **2014**, *5*, 3825.
[37] E. Kemppainen, A. Bodin, B. Sebok, T. Pedersen, B. Seger, B. Mei, D. Bae, P. C. K. Vesborg, J. Halme, O. Hansen, P. D. Lund, I. Chorkendorff, *Energy Environ. Sci.* **2015**, *8*, 2991 – 2999.
[38] G. W. Busser, B. Mei, M. Muhler, *ChemSusChem* **2012**, *5*, 2200 – 2206.
[39] G. W. Busser, B. Mei, A. Pougin, J. Strunk, R. Gutkowski, W. Schuhmann, M.-G. Willinger, R. Schlögl, M. Muhler, *ChemSusChem* **2014**, *7*, 1030 – 1034.
[40] X. Wang, Q. Xu, M. Li, S. Shen, X. Wang, Y. Wang, Z. Feng, J. Shi, H. Han, C. Li, *Angew. Chem. Int. Ed.* **2012**, *51*, 13089 – 13092; *Angew. Chem.* **2012**, *124*, 13266 – 13269.

Manuscript received: September 20, 2017
Revised manuscript received: October 26, 2017
Accepted manuscript online: October 26, 2017
Version of record online: November 10, 2017